engineering proceedings

MDPI

Proceedings Paper

Multi-Parametric Analysis of a Mimicked Accelerating Pedal (Via DC Motor) of an Electric Vehicle †

Hassan Niaz, Muhammad Abdullah Sheeraz * and Muhammad Ahsan Naeem

Department of Mechatronics and Control Engineering, University of Engineering and Technology, Lahore 54890, Pakistan; 2020mc30@student.uet.edu.pk (H.N.); email1@email.com (M.A.N.)

* Correspondence: abdullahtlg8@gmail.com

† Presented at the 4th International Electronic Conference on Applied Sciences, 27 October–10 November 2023; Available online: https://asec2023.sciforum.net/.

Abstract: In this 21st century, researchers have been exploring different designs, performance characteristics, charging-discharging regions, and regenerative braking aspects of electric vehicles. However, there has been a major gap in the multimodal analysis of the accelerating pedal drive for electric vehicles; therefore, herein, the novel analytical model of a mimicked foot pedaling control of the electric vehicle is developed by cascading five sub-models (i.e., Foot Pedal, Resistive Potentiometer, 555-Timer, Buck-Converter, and the permanent magnet DC Motor) to synthesize the overall 3rd order transfer function of the system. MATLAB is utilized to comprehensively analyze the transient and steady-state characteristics of the developed model by considering the Pedaling force, four different materials (i.e., Aluminum, Brass, Carbon Fiber, Polyamide 6), Potentiometer's resistance, mechanical and electrical attributes of the motor. Results highlight that the linear pedaling drive is possible by considering Polyamide 6 material at pedaling properties of 0.25 kg Mass and 2.679 Ns/m Damping Coefficient. Furthermore, at a lesser potentiometer track length (around 10 cm) and equivalent inertia of 5 Kgm^2, the motor generates the regulated angular velocity, thereby minimizing the transient characteristics in the accelerating pedal.

Keywords: electric vehicles; accelerating pedal; Polyamide-6; steady-state; transfer function

Citation: Niaz, H.; Sheeraz, M.A.; Naeem, M.A. Multi-Parametric Analysis of a Mimicked Accelerating Pedal (Via DC Motor) of an Electric Vehicle. *Eng. Proc.* **2023**, *52*, x. https://doi.org/10.3390/xxxxx

Academic Editor(s): Name

Published: date

1. Introduction

With the recent advancements in sustainable transportation, electric vehicles (EVs) have been emerging as a promising solution to mitigate environmental impacts primarily due to their lesser emissions, overall efficiency, and reduced dependency on fossil fuels [1,2]. Miniaturized elements have been introduced to EVs to improve the safety of both passengers and pedestrians. Different renewable energy harvesting techniques [3,4] are being explored for ultra-low power electronics of electric vehicles. Researchers have been working on several sub-domains of electric vehicles to evaluate the performance of the newly designed vehicles [5]. The ideation of emerging vehicles is started from the modeling and the scientific community has been working on individual models of batteries, power converters, engine power distributions, and actuators which in turn helps us to visualize the dynamics of EVs. The braking action in EVs is optimized by implying neural networks and state-of-the-art control schemes for Intelligent Braking Systems [6].

The control of Electric Vehicles is highly influenced by the individual characteristics of the accelerating pedal. However, the performance of the accelerating pedal drive is inadequately available in the literature [6–8]; therefore, in this research work, a novel analytical model of the pedaling control of an EV is developed and further numerically analyzed under various conditions of the controllable factors. In this paper, Section 2 presents the analytical model, Section 3 gives insights into the results obtained and finally, Section 4 concludes the paper along with future recommendations.

2. Analytical Model

In this section, the proposed system, shown in Figure 1, has been modeled based on the classical yet concatenated approach in which the pedaling force is utilized to configure the 555 Timer in astable mode for generating a wave of the desired duty cycle. This controllable square wave produces the targeted output voltage for controlling the DC motor.

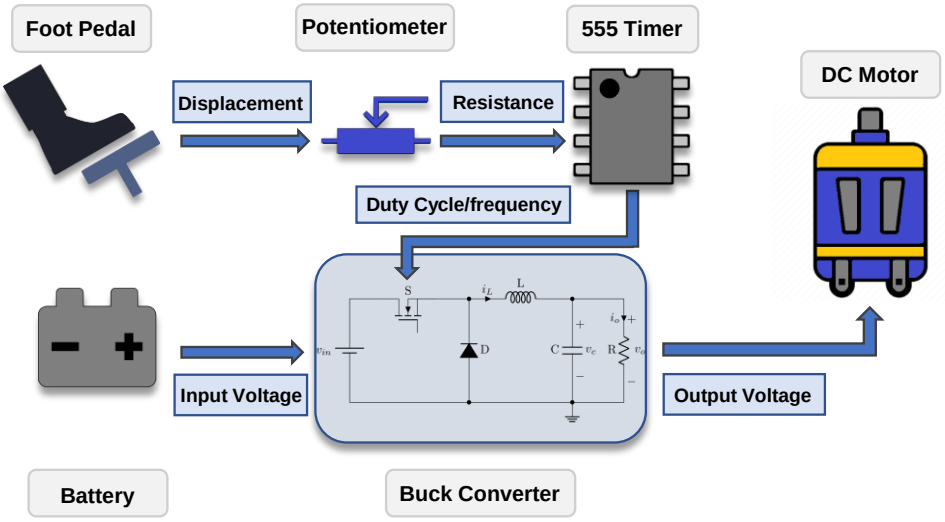

Figure 1. Schematic of the Mimicked Accelerating Pedal of EV.

The mimicked accelerating pedal has been modeled by considering the multiparametric relationships between the above-mentioned sub-systems and therefore, prominent parameters of the overall model are given in Table 1.

Table 1. Parameters of the proposed system [9,10].

Mechanical Parameters	Units	Values	Electrical/Electromechanical Parameters	Units	Values
Mass of pedal (m)	kg	0.25	Potentiometer Resistance (R_1)	Ω	1000
Damping Coefficient of Pedal (b)	N-s/m	2.679	555-timer Resistance (R_2)	Ω	50
Foot Pedal Stiffness (K_2)	N/m	100	Input Battery Voltage (V_{in})	V	50
Area of Pedal (A_o)	cm^2	400	Motor Toque Constant (K_t)	Nm/A	1
Load Inertia (J_{eq})	Kgm^2	7	Motor Back Emf Constant (K_b)	Vs/rad	0.1
Load Damping (D_{eq})	Nms/rad	1	Armature Resistance (R_a)	Ω	1

The pedal system is modeled by an equivalent mass spring damper system with combined stiffness ($k = k_1*k_2/k_1 + k_2$) as shown in Figure 2a,b in which k_1 is the pedal stiffness ($k_1=\frac{F}{x}=\frac{EA_o}{L_o}$), and subsequently, the transfer function is given by Equation (1). Due to this change in displacement (X(s)), the change in sider resistance (R_{1a}) will be noticed as shown in Figure 2c, and the resultant equation for depicting this change in resistance concerning the displacement is given by Equation (2).

$$\frac{X(s)}{F(s)}=\frac{1}{ms^2+bs+k} \quad (1)$$

$$\frac{R_{1a}(s)}{X(s)}=\frac{R_1}{L} \quad (2)$$

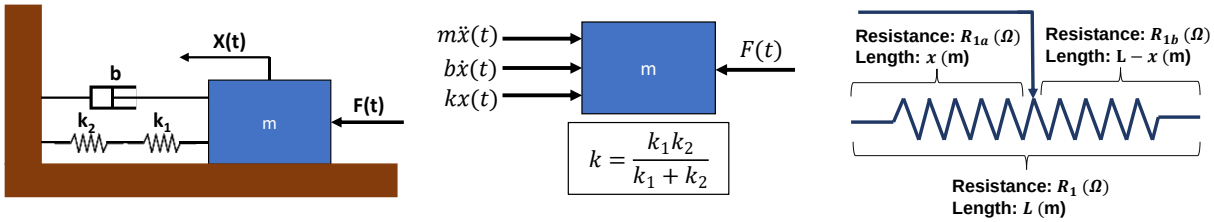

(**a**) (**b**) (**c**)

Figure 2. (**a**) General schematic of the foot pedal sub-system; (**b**) Free Body Diagram of the foot pedal sub-system; (**a**) General schematic of the potentiometer sub-system.

In the conventional models of the 555 Timer in astable mode, the frequency is also influenced by regulating the duty cycle which is undesirable (In our proposed system) as it will disturb the operation of the buck converter in Continuous Conduction Mode (CCM) [5]. Therefore, a different configuration of 555 Timer is proposed by introducing diodes in which the frequency remains constant with the variations in the duty cycle as shown in Figure 3, and modified equations for this sub-system (555-timer) are given below:

$$T_{hi} = \ln(2) * (R_{1a} + R_2)C_1;\ T_{low} = \ln(2) * R_{1b}C_1 \quad (3)$$

$$f = \frac{1}{\ln(2) * (R_1 + R_2)C_1};\ D(t) = \frac{R_{1a}(t) + R_2}{R_1 + R_2} \quad (4)$$

where R_1 is the resistance of the potentiometer sub-system. Taking the Laplace transform of Equation (4) with the assumption that $\mathbf{R_1 >> R_2}$ yields the following transfer function:

$$\frac{D(s)}{R_{1a}(s)} = \frac{1}{R_1 + R_2} \quad (5)$$

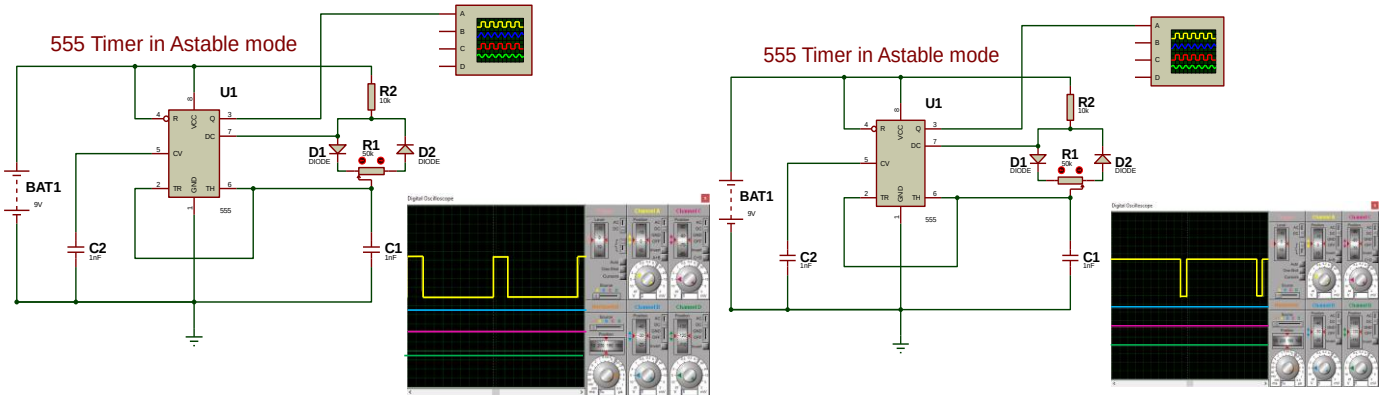

(**a**) (**b**)

Figure 3. Simulation results of the proposed 555 timer sub-system with (**a**) Potentiometer resistance (R_{1a}) nearly equal to zero; (**b**) Potentiometer resistance (R_{1a}) nearly equal to the maximum resistance.

After analyzing the duty cycle, the buck converter (due to its switching characteristics) has further been considered in two distinct cases: When the input switch is closed (from 0 to DT seconds) and when the input switch is opened (from DT to T seconds) as given below [9].

$$i_L(DT) = i_L(0) + \frac{1}{L_b}\int_0^{DT} (V_{in} - V_{out})\, dt \quad (6)$$

$$i_L(T) = i_L(DT) + \frac{1}{L_b}\int_{DT}^{T} -V_{out}\,dt \tag{7}$$

In the proposed system, the buck converter is in CCM with a constant duty cycle and an average output current [5], therefore, the model equations will be reduced to:

$$\frac{V_{out}(s)}{D(s)} = V_{in} \tag{8}$$

The final sub-system is the electromechanical motor, powered by the output voltage (V_{out}) of the buck converter and can be modeled by Equation (9).

$$V_{out}(t) = \frac{T_m(t)}{k_t}R_a + k_b\omega_m(t);\ T_m(t) = J_{eq}\frac{d\omega_m}{dt} + D_{eq}\omega_m(t);\ \frac{\omega_m(s)}{V_{out}(s)} = \frac{k_t}{R_a\left(J_{eq}s + D_{eq}\right) + k_t k_b} \tag{9}$$

Finally, the transfer function of the overall system is the product of the transfer functions of each subsystem.

$$\frac{\omega_m(s)}{F(s)} = \frac{X(s)}{F(s)} * \frac{R_{1a}(s)}{X(s)} * \frac{D(s)}{R_{1a}(s)} * \frac{V_{out}(s)}{D(s)} * \frac{\omega_m(s)}{V_{out}(s)} \tag{10}$$

Using Equations (1), (2), (5), (8) and (9) the final form of the 3rd-order transfer function is

$$\frac{\omega_m(s)}{F(s)} = \frac{k_t V_{in} R_1}{L(R_1 + R_2)\left[R_a J_{eq} m s^3 + \left(R_a J_{eq} b + R_a D_{eq} m + k_t k_b m\right)s^2 + \left(R_a J_{eq} k + R_a D_{eq} b + k_t k_b b\right)s + (R_a D_{eq} k + k_t k_b k)\right]} \tag{11}$$

3. Results and Discussions

In this section, the results of the multi-parametric analysis (using MATLAB) of the mimicked accelerating EV Pedal are presented to evaluate the response under different values of controllable factors. Figure 4 highlights the steady-state angular speed of the motor for different types of pedal materials (Aluminum, Brass, Carbon Fiber, and Polyamide-6) under four different applied forces. The results depict that Polyamide-6 is the superior material, as it yields the largest steady-state angular velocity compared to the other materials (As illustrated in the magnified section of Figure 4). This is because, under the same parametric conditions, Polyamide-6 generates the largest deflection. This outcome validates the theoretical interpretations from the literature which signifies that polyamide-6 is the main material for the automotive industry, specifically for the manufacturing of Pedal [11].

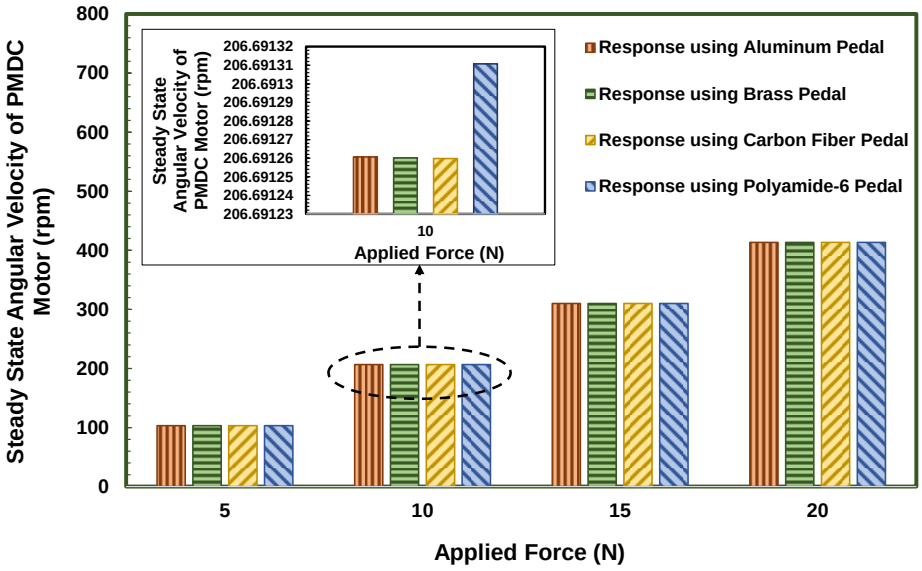

Figure 4. Steady-state responses for different pedal materials under variance in the applied force.

Figure 5a shows the trend of the steady-state angular speed of the motor for different excitation forces, variant potentiometer resistances, and by considering the constant length of the potentiometer track. Results emphasize the existence of a positive correlation between the response and potentiometer resistance, making the 10 kΩ potentiometer a suitable option. This is because, at this higher potentiometer resistance (10 kΩ), the duty cycle increases due to the traversal resistance (R_{1a}) as given by Equation (5) which consequently enhances the overall response of the system.

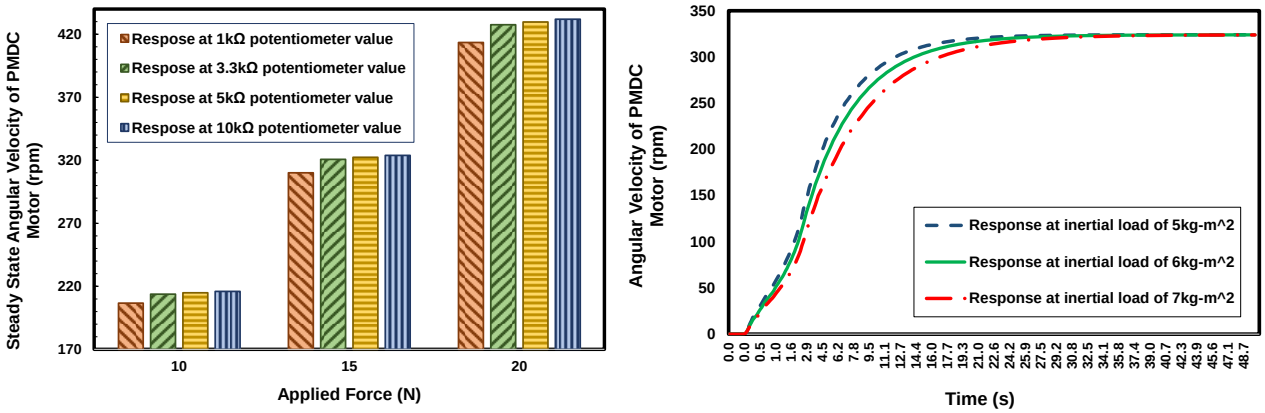

(**a**) (**b**)

Figure 5. (**a**) Comparison between steady-state responses of the model using different potentiometers; (**b**) Effects of different inertial loads on the time-varying speed response of the model.

The time-varying response of Polyamide-6 at an average force of 15 N is further evaluated by considering the different inertial loads as shown in Figure 5b. In the system of higher inertial loads, the settling time of the motor would be greater, and therefore, for the given mimicked system, an inertia of 5 kg/m^2 is desirable.

After selecting the desirable potentiometer resistance, pedal material, and inertial load, the response (Steady State as well as transient) has further been investigated by considering different armature resistances as shown in Figure 6. It can be seen that a motor with a smaller value of armature resistance produces greater steady-state speed. The reason is that by increasing the armature resistance, the voltage drop across the resistor increases which decreases the voltage which is to be converted in the rotational motion. The result of this analysis aligns with the research conducted by [10] in which they investigated speed control techniques for a DC motor.

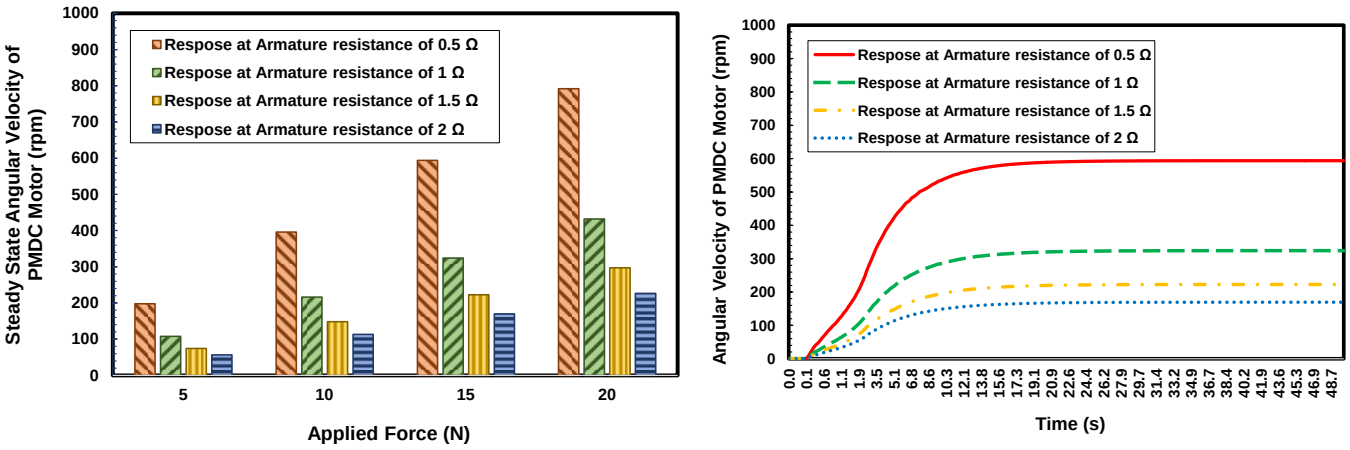

(**a**) (**b**)

Figure 6. Response of the system with the variations in armature resistances. (**a**) Steady State (**b**) Time-varying response under a constant force (15 N).

The dynamic response is further validated by considering the impulse test signal of different magnitudes (5 N, 10 N, 15 N) as shown in Figure 7. Results highlight that for any test signal magnitude, the sensitivity of the proposed system is 0.1317 rpm/N, justifying the meaningful change in the angular motion due to the pedal displacement (Excitation force). Additionally, this test signal is applied only for 0.01 s and the model produces a reasonable steady state angular velocity (Peak Output) of 0.6585 rpm at the minimum applied force of 5 N as given in Table 2. Results further highlight that irrespective of the magnitude of the test signal, the model generates the peak output around 0.170 s, signifying the regulated response time.

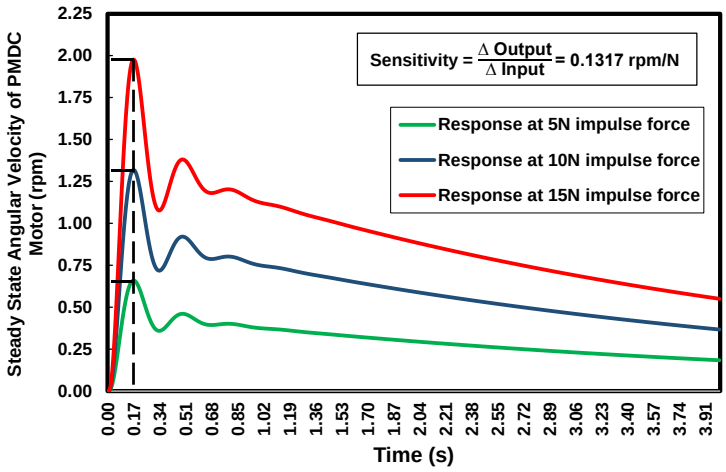

Figure 7. Response of the system for instantaneous impulse inputs.

Table 2. Response Time via variant signal magnitudes.

Impulse Magnitude (N)	Peak Output Response (rpm)	Time (s)
5	0.6585	0.170
10	1.3171	0.170
15	1.9756	0.170

4. Conclusions

In this research work, a comprehensive analysis has been presented to evaluate the performance of the mimicked accelerating pedal by considering variations in the pedal materials, potentiometer resistance, excitation force, armature resistance, and inertial loads. Results highlight that Polyamide-6 is the best pedal material for the pedaling action in an electric vehicle due to its adaptability with the excitation forces. Furthermore, the proposed model generates a maximum steady state angular speed of the motor for a pedal of 0.25 kg mass, a potentiometer of 10 kΩ resistance, minimum inertial load (5 kg/m^2), and an armature resistance of 0.5 Ω. Based on the results obtained and under these targeted parametric values, the motor can rotate at a speed of ~70 km/h (assuming a wheel of 18 in. diameter) with 20 N excitation force. The output response due to the different magnitudes of the test signal justifies the sensitivity of the system as 0.1317 rpm.

Author Contributions: Conceptualization, H.N. and M.A.S.; methodology, H.N.; software, H.N.; validation, H.N. and M.A.S.; formal analysis, H.N., M.A.S. and M.A.N.; investigation, H.N. and M.A.S.; resources, H.N. and M.A.S.; data curation, H.N.; writing—original draft preparation, H.N.; writing—review and editing, M.A.S.; visualization, H.N. and M.A.S.; supervision, M.A.S.; project

administration, M.A.S. and M.A.N.; funding acquisition, M.A.S. and M.A.N. All authors have read and agreed to the published version of the manuscript.

Funding: This research received no external funding.

Institutional Review Board Statement:

Informed Consent Statement:

Data Availability Statement:

Conflicts of Interest: The authors declare no conflict of interest.

References

1. Sanguesa, J.A.; Torres-Sanz, V.; Garrido, P.; Martinez, F.J.; Marquez-Barja, J.M. A Review on Electric Vehicles: Technologies and Challenges. *Smart Cities* **2021**, *4*, 372–404.
2. Mosin, M.; Popov, N.; Anibroev, V.; Vilberger, M.; Domakhin, E. Engine Power Distribution System for Four-Wheel Drive Autonomous Electric Vehicle. *Energy Rep.* **2023**, *9*, 115–122.
3. Sheeraz, M.A.; Malik, M.S.; Rahman, K.; Elahi, H.; Khurram, M.; Eugeni, M.; Gaudenzi, P. Multimodal Piezoelectric Wind Energy Harvester for Aerospace Applications. *Int. J. Energy Res.* **2022**, 46, 13698–13710.
4. Sheeraz, M.A.; Malik, M.S.; Rehman, K.; Elahi, H.; Butt, Z.; Ahmad, I.; Eugeni, M.; Gaudenzi, P. Numerical Assessment and Parametric Optimization of a Piezoelectric Wind Energy Harvester for IoT-Based Applications. *Energies* **2021**, *14*, 2498.
5. Rashid, M.H. *Power Electronics Handbook*; Butterworth-Heinemann: Oxford, UK, 2017.
6. He, H.; Wang, C.; Jia, H.; Cui, X. An Intelligent Braking System Composed Single-Pedal and Multi-Objective Optimization Neural Network Braking Control Strategies for Electric Vehicle. *Appl. Energy* **2020**, *259*, 114172.
7. Prajwowski, K.; Golebiewski, W.; Lisowski, M.; Abramek, K.F.; Galdynski, D. Modeling of Working Machines Synergy in the Process of the Hybrid Electric Vehicle Acceleration. *Energies* **2020**, *13*, 5818.
8. Tran, D.-D.; Vafaeipour, M.; El Baghdadi, M.; Barrero, R.; Van Mierlo, J.; Hegazy, O. Thorough State-of-the-Art Analysis of Electric and Hybrid Vehicle Powertrains: Topologies and Integrated Energy Management Strategies. *Renew. Sustain. Energy Rev.* **2020**, *119*, 109596.
9. Kaur, R.; Kaur, N. Mathematical Modelling of Buck Converter. *Int. J. Recent Innov. Trends Comput. Commun.* **2014**, *2*, 1226–1229.
10. Ayasun, S.; Karbeyaz, G. DC Motor Speed Control Methods Using MATLAB/Simulink and Their Integration into Undergraduate Electric Machinery Courses. *Comput. Appl. Eng. Educ.* **2007**, *15*, 347–354.
11. Bernasconi, A.; Rossin, D.; Armanni, C. Analysis of the Effect of Mechanical Recycling upon Tensile Strength of a Short Glass Fibre Reinforced Polyamide 6, 6. *Eng. Fract. Mech.* **2007**, *74*, 627–641.